1-1-2018

Fe-doped phosphorene for the nitrogen reduction reaction

Zengxi Wei
Hunan University

Yuefeng Zhang
Hunan University

Shuangyin Wang
Hunan University

Caiyun Wang
University of Wollongong, caiyun@uow.edu.au

Jianmin Ma
Hunan University

Fe-doped phosphorene for the nitrogen reduction reaction

Abstract

The nitrogen-to-ammonia conversion is one of the most important and challenging processes in chemistry. We have employed spin-polarized density functional theory to propose Fe-doped monolayer phosphorene (Fe-P) as a new catalyst for the N2reduction reaction at room temperature. Our results show that single-atom Fe is the active site, cooperating with P to activate the inert N-N triple bond and reduce N2to NH3via three reliable pathways. Our findings provide a new avenue for single atom catalytic nitrogen fixation under ambient conditions.

Disciplines

Engineering | Physical Sciences and Mathematics

Publication Details

Wei, Z., Zhang, Y., Wang, S., Wang, C. & Ma, J. (2018). Fe-doped phosphorene for the nitrogen reduction reaction. Journal of Materials Chemistry A, 6 (28), 13790-13796.

Fe-doped Phosphorene for Nitrogen Reduction Reaction

Zengxi Wei,[a] Yuefeng Zhang,[a] Shuangyin Wang,[b,]* Caiyun Wang[c] and Jianmin Ma[a,]*

[a]*School of Physics and Electronics, Hunan University, Changsha 410082, P. R. China*

[b]*State Key Laboratory of Chem/Bio-Sensing and Chemometrics, College of Chemistry and Chemical Engineering, Hunan University, Changsha, P. R. China*

[c]*ARC Centre of Excellence for Electromaterials Science, Intelligent Polymer Research Institute, AIIM Facility, University of Wollongong, North Wollongong, NSW 2500, Australia*

Corresponding authors: Shuangyin Wang or Jianmin Ma

E-mail: shuangyinwang@hnu.edu.cn (S.Y. Wang)
nanoelechem@hnu.edu.cn (J.M. Ma)

Abstract

The nitrogen-to-ammonia conversion is one of the most important and challenging process in chemistry. We have performed spin-polarized density functional theory to propose Fe-doped monolayer phosphorene (Fe-P) as a new catalyst for N_2 reduction reaction at room temperature. Our results show that the single-atom Fe is the active site, cooperating with P to activate the inert N-N triple bond and reduce N_2 into NH_3 via three reliable pathways. Our findings provide a new avenue for single atom catalytic nitrogen fixation under ambient conditions.

Keywords: Nitrogen reduction; Electrocatalysis; Phosphorene; Single-atom doping; Atomic Iron

1. Introduction

Converting the abundant nitrogen (N_2) in the Earth's atmosphere to ammonia (NH_3), which is so-called nitrogen fixation, is one of the most attractive conversions in biochemistry.[1-4] To overcome the inertness of N_2 molecules, tremendous efforts have been devoted to identify the feasible catalytic systems for this transformation [5-7]. Generally, the industrial fixation of N_2 is via the Haber-Bosch process, which is primarily used for production of fertilizers.[8, 9] However, the Haber-Bosch process consume huge amount of energy, which requires high temperatures and high pressures of reactants N_2 and H_2 gases with the aid of Fe or Ru catalysts to break the inert triple bond of N_2.[10-14] In contrast, the biological N_2-fixation, under ambient conditions, through the nitrogen-binding enzymes called nitrogenases to activate the N-N bond of N_2.[4, 11, 15-20] It is essential that the nitrogen fixations through the catalysts of nitrogenases undergo six sequential process of protonation and electron transfers. In addition, the N-N triple bond of N_2 have been not cleavaged to adatoms at the first step of the reduction process.

Reduction of dinitrogen at the most successful nitrogenases occurs at a FeMo cofactor, which consists of two fused iron-sulfur clusters and can additionally contain Mo and/or V atoms,[16, 19, 21-27] but the detailed mechanism remains unexplored. Further, molecular catalysts have been developed by imitating the biological N_2-fixation.[2, 16, 21, 28, 29] They are rather promising catalysts for the reduction reaction of N_2 that can occur under flexible temperature and pressure. Especially, the product NH_3 can be extracted friendly from the hydrogen feed gas, and possessing the adjustable operating potential, pH, electrolyte, etc., enhancing the production yield of NH_3 dramatically.

It is a remarkable fact that transition metals (TMs) play an indispensable role in this catalytic system, especially the element Fe.[24, 30-37] For example, Rodriguez et al.[30]

propose an iron-potassium system as a support for the N_2-fixation, Li et al.[35] propose FeN_3-embedded graphene as the catalyst for nitrogen fixation, Hu et al.[36] present Fe^{3+}@C_3N_4 can activate the N_2 molecule effectively. Their results suggest that Fe atom in the N_2-fixation process plays a key role.

Phosphorene, a monolayer of black phosphorous (P), has recently received much attention owing to its novel properties, such as promising electronic properties and high carrier mobility. It has found wide applications in[38, 39] electronics, optoelectronics, solar cells, and catalysts.[40-44] Although tremendous progress has been made in the research of P, there are few reports about its application in electrocatalysis. In particular, using P as the electrocatalyst for electrocatalytic dinitrogen fixation under ambient conditions have not been reported.

Here, we hypothesis that single atom Fe-doped P (Fe-P) can imitate nitrogenases to catalyze N_2-fixation from first-principles calculations. Our works illustrate that both P and Fe-P have the capacity of N_2-fixing. Especially, Fe-P can activate the N_2 distinctly than P because it can release energy when N_2 is adsorbed on the surface of Fe-P. Moreover, every step is actually exothermic during the reaction process of dinitrogen to ammonia.

2. Computational methods

All calculations are based on the spin-polarized density functional theory (DFT) methods by using the Cambridge Serial Total Energy Package (CASTEP) code on the basis of the plane-wave pseudopotential. The Perdew-Burke-Ernzerhof (PBE) exchange-correlation functional for generalized gradient approximation (GGA)[45] was employed to optimize all the geometric structures. The van der Waals interaction were applied within the Grimme scheme. The cut-off energy was set to 450 eV with a

Brillouin zone was sampled by a Monkhorst-Pack 5×5×1 K-point grid.[46] The process of geometry optimization approached the electronic ground state when the energy and force on each ion were reduced below 10^{-6} eV and 0.01 eV/Å. HSE06 calculations was performed to get the exact band structure for P. The band gap is 0.92 eV for GGA/PBE, and 1.61 eV for HSE06 methods. The band gap of HSE06 calculations was comparatively accurate to the experimental and theoretical results.[47, 48] To model the Fe-P structure, we first built a periodic supercell (3×3) containing 38 P atoms with a vacuum of 15 Å in the z-direction. And then, Fe atom anchored on the channel of P, but do not remove any P atom at all. Fortunately, we find that the binding energies of Fe was -6.88 eV with the cohesive energy of atomic Fe and was -4.17 eV with bulk Fe, which is implied that a Fe atom could be anchored in the channel of P. The reaction energy was calculated by using the equation:

$$\Delta E = E(\text{Fe-P-N}_2\text{H}_X) - E(\text{Fe-P-N}_2\text{H}_{X-1}) - E(\text{H}^+) - E(\text{e}^-)$$

where $E(\text{Fe-P-N}_2\text{H}_X)$ and $E(\text{Fe-P-N}_2\text{H}_{X-1})$ are the adsorption energy after and before the protonation process, $E(\text{H}^+)$ and $E(\text{e}^-)$ represent the energy of proton and electron, respectively. The energies of proton and electron were based on the model of Lutidinium ($[\text{LutH}]^+$) and [CoCp*$_2$], and the total energy of proton and electron was ca. -14.70 eV in our work.[49] The adsorption energy (E_{ad}) was defined as follows:

$$E_{ad} = E_{F-P/N_2H_X} - E_{F-P} - E_{N_2H_X}$$

where E_{F-P/N_2H_X}, E_{F-P}, and $E_{N_2H_X}$ are the total energies of F-P with adsorbate, a clean surface of F-P, and the isolated adsorbate of N_2H_X, respectively.

3. Results and discussion

The optimized lattice parameter of the P predicted in this study is a = 4.62 Å and b = 3.28 Å (inset of rectangle in **Figure 1**b), which agrees well with the experimental results.[50-53] The top view of the P has shown that the thickness of P was ca. 2.08 Å (**Figure 1**a). The P-P bond length of top and down layer was 2.20 Å and 2.24 Å for the interlayer length (**Figure 1**b). For Fe-P, the embedded Fe in the channel of P is shown in **Figure 1**c and d. After the doping of Fe, its adjacent P atom in the top layer upward movement and the opposite P atom in the down layer moved down lightly. The maximum thickness of Fe-P was 3.36 Å, which is bigger than that of P. Compared with the parameter of P, we have shown the changes of relative bond length of Fe-P in the **Table S**1.

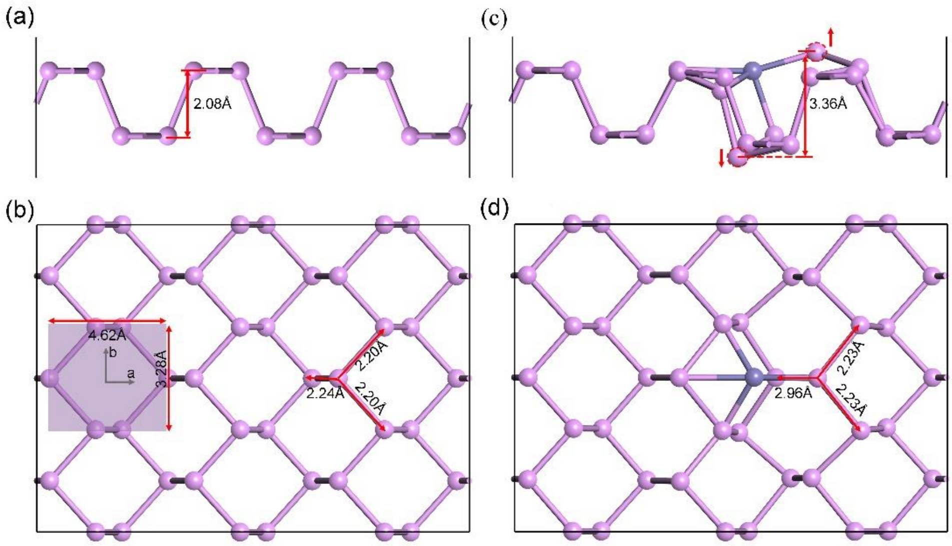

Figure 1. Optimized structure of (a) top and (b) side view of the (3×3) P supercell. The inset of rectangle represents the lattice constants of the unit cell of P and the relevant bond length and angles are emphasized with red arrows. Top (c) and side view (d) of the Fe-P with the relevant parameters. Pink and gray balls represent the P and Fe atoms, respectively.

The electronic properties, such as bandgap, charge, molecule orbitals and spin density distribution of P and Fe-P were studied. These properties were vital for catalysts to facilitate N_2 adsorption and activate its inert N-N triple bond. Recently research has shown that the bandgap of P was cat. 1.5-1.6 eV by using the hybrid functional (HSE06) methods, which agrees with relative experimental reports.[48] However, the generalized gradient approximation methods will underestimate the bandgap of P about 50%. From the density of states and band structure (as shown in **Figure S1**a and b), we can see that the bandgap of P was 1.61 eV by using the HSE06 and 0.92 eV for the GGA methods. Additionally, the P has a direct bandgap because both valance band maximum and conduction band minimum are located in the same high symmetry points G, which is in accordance with recent reports.[48, 54, 55] After doping Fe, the bandgap of Fe-P is decreasing to 0.65 eV with an indirect bandstructure (as shown in Figure S2a and b). We can find that both GGA and HSE06 functionals have the same bandstructure, and we shew one of them in Figure S2. The indirect bandgap between the high symmetry points G and F, as shown in Figure S2b, which is conducive to transfer charges from Fe-P to adsorbate and activate the adsorption.

According to the Mulliken population analysis (as shown in **Table S**2), the Fe atom lose 0.18 e and the charges of adjacent P atoms had been recombined. The P_1, P_4, P_7, P_8 and P_{11} gained 0.12 e, 0.07 e, 0.07 e, 0.03 e and 0.03e, respectively. On the contrary, the P_2, P_3, P_5 and P_6 missed 0.04 e, 0.03 e, 0.03 e and 0.03e, respectively. We can find that the charges of Fe was transferred to the whole P. Further, the Bader charge analysis elucidated that the P got 0.18 e from the doped F atom, which is work in concert with the Mulliken population analysis results.

Additionally, from the highest occupied molecular orbitals (HOMO) of P implied that there is a symmetrically distributed electron delocalization (**Figure 2**a), but the electron was located on the Fe atom of Fe-P (**Figure 2**b). The presence of Fe also introduced asymmetric charge and spin density distribution throughout the ground state geometry resulting in a high spin density (**Figure 2**c and d). The positive spin density on Fe atom clearly indicates that Fe atom is catalytically active and effective for chemisorption. This makes Fe-P a potential candidate for the electrocatalytic N_2 reduction.

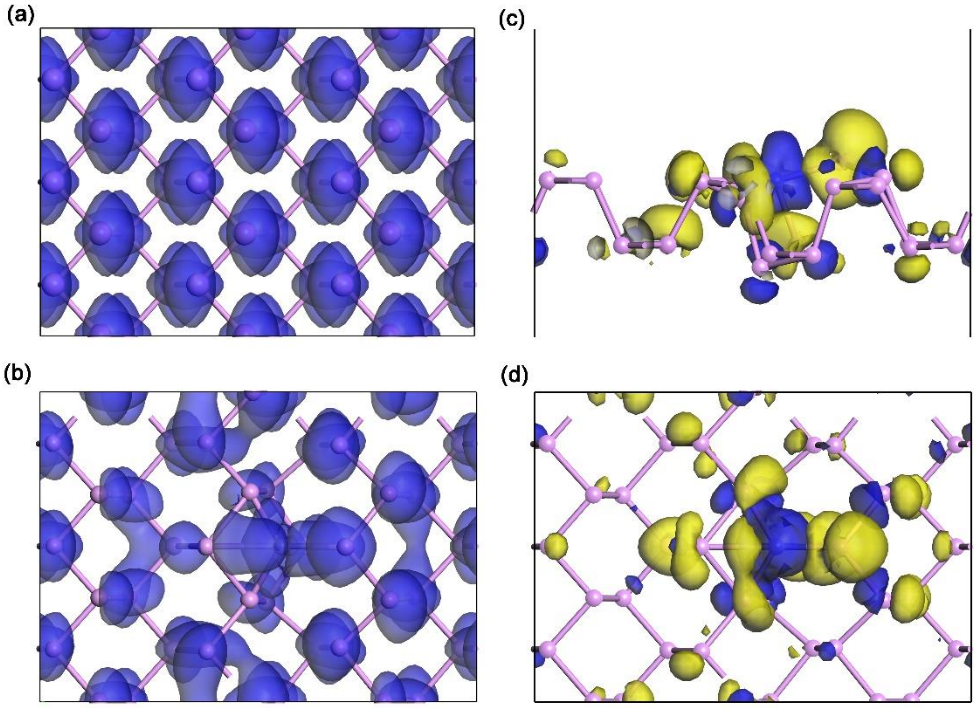

Figure 2. The highest occupied molecule orbitals of (a) P and (b) Fe-P. (c) Side view and (d) top view of spin density distribution. Blue and yellow isosurfaces mean positive and negative spin density, respectively.

It is well-recognized that the first step of the electrocatalytic N_2 reduction reaction is the adsorption of N_2 on the catalyst surface. Also this adsorption plays an important role in the subsequent reaction pathways. Once it is adsorbed on the catalyst surface and activated, the reaction process can be realized at room temperature. We discuss the N_2 adsorption on the P and Fe-P surface in details.

After the structural relaxation, N_2 molecule cannot adsorb onto the surface of P, but the Fe-P surface with Fe atom doping. Our results show that the adsorption energy was -0.81eV, and we can confirm the chemisorption occured on the surface of Fe-P. The bond length of N-N triple bond was changed subsequently, the triple bond was increased to 1.17 Å for single-contact and 1.19 Å for double- contact. However, the N-N triple bond did not change and maintained the free N-N bond length of 1.15 Å. Only weak physical adsorption occurred on the surface of P with an adsorption energy of

2.75 eV. These results suggest that Fe-P have a prominent ability to activate inert N-N triple bond.

To reveal the genuine interaction between nitrogen molecule and catalyst surface, we have calculated the density of states (DOS) and shown in **Figure 3**. For free nitrogen molecule (**Figure 3**a), the orbitals of N_2 are $\sigma_g 2s$, $\sigma_\mu {}^* 2s$, $\pi_\mu 2p$, $\sigma_g 2p$ and $\pi_g {}^* 2p$ are located at -17.78 eV, -3.85 eV, -1.26 eV and 0.00 eV, -7.27 eV, respectively. Moreover, the highest occupied molecule orbital (HOMO) and the lowest unoccupied molecular orbital (LUMO) is located at $\sigma_g 2p$ and $\pi_g {}^* 2p$, respectively. Thus, we can obtain the bandgap of N_2 and it was 8.53 eV, which agrees with the relevant reports.[36] The large energy gap between the HOMO and LUMO makes proton and electron transfer reaction difficult, which is one of the main hurdles in N_2 fixation. The inert N_2 needs to be activated by catalyst to produce ammonia. We have found that the orbitals of N_2 in N_2-P (**Figure 3**b) were the same as free nitrogen molecular orbitals, indicative of a weak N_2 activation ability of P. Fortunately, both of SN-C (**Figure 3**c) and DN-C (**Figure 3**d) fashions are enforcing the delocalized electrons of $\sigma_g 2p$ orbitals significantly. The overlap of orbitals between $\sigma_g 2p$ and $\pi_g {}^* 2p$ verified the potent activation ability of Fe-P for the dinitrogen-to-ammonia conversion at ambient temperature.

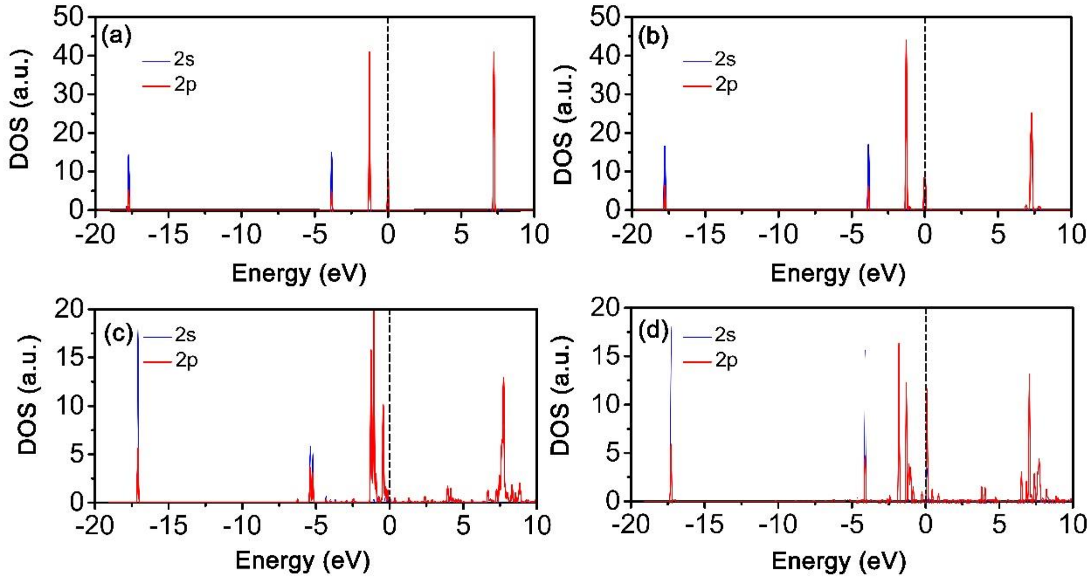

Figure 3. Density of states of s and p orbitals of N_2. (a) Free nitrogen molecule, (b) N_2 adsorbed on P, (c) and (d) N_2 adsorbed on Fe-P with SN-C and DN-C fashion, respectively. The Fermi level is set to zero.

We also calculated the charge density difference to imitate the electrons transfer behavior as shown in **Figure 4.** The blue and yellow isosurfaces represent charge accumulation and depletion in the three-dimensional space, respectively. When N_2 was adsorbed on P, the faint depletion (mapped with yellow isosurfaces, **Figure 4**a and b) of electrons between two N atoms elucidated that P can reduce the bond energy of N-N triple bond slightly (as shown in **Table S3**). However, we have found that plenty of electrons accumulate on the surface of two N atoms and a depletion of electrons between two atoms apparently (**Figure 4**c and d). In particular, the DN-C fashion (**Figure 4**e and f) can make the most electron of Fe-P transfer to N_2 molecular and activate the N-N triple bond extremely.

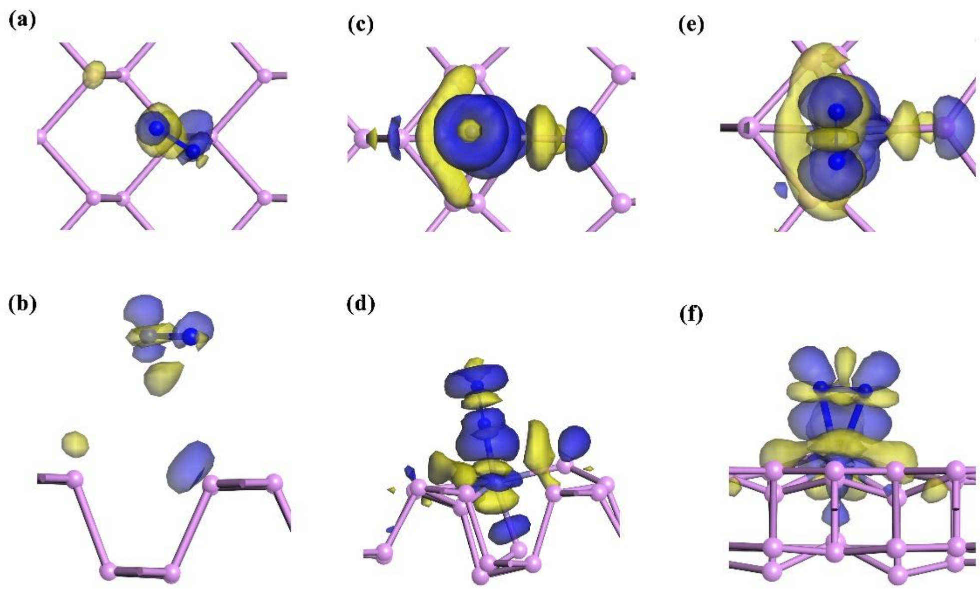

Figure 4. The charge density difference of N_2 molecule adsorbed on the surface: (a) Top view and (b) side view of P. (c,d) Top view and side view of Fe-P, the status of N_2 is single N atom contact (SN-C). (e, f) top view and side view of double N atom contact (DN-C) on Fe-P surface. The blue and yellow isosurfaces represent charge accumulation and depletion in the three-dimensional space, respectively.

To further evaluate the conversion mechanism of activated dinitrogen to ammonia on P-based catalysts, we canvassed the whole six proton/electron reduction process undergo three possible pathways, including the distal (abbreviated as 'Dis'), alternating (abbreviated as 'Alt') and enzymatic (abbreviated as 'Enz') as shown in **Figure 5**. The optimized geometry structures of all the reduction process are displayed in **Figure S3.** From the N_2-adsorption and N_2-release, there are eight steps for each pathway (e.g. Dis, Alt and Enz pathways). We find that P is only undergoing the Dis pathway (**Figure 5**a). The cleavage of N-N triple bond occurred at the fourth step with release of an NH_3, and the second ammonia was released in the eighth step. Finally, P was regenerated, suggesting the feasibility of the N_2 reduction reaction process. For Fe-P, both the Dis and Alt pathways undergoing in our expectation, but the Enz pathway is an exception. It released the intermediate product N_2H_4 at the fifth step ($*NH_2\text{-}HN* \rightarrow NH_2\text{-}NH_2$), as shown in **Figure** S4. A strong acidic environment may the hinder of emitting N_2H_4 gas and obtain the main product ammonia. Thus, we hypothesis that the protonation process of Enz pathway at the fourth step can form a NH* species in the Dis pathway and/or H_2N-H_2N* species in the Alt pathway, respectively. From *NH_2-HN* to NH_2-NH_2, HN*+NH_3 and H_2N-H_2N*, the reaction energy in the ascending order was -1.06 eV, -1.67 eV and -2.34 eV, respectively (**Figure S5**). It can be concluded that the optimal scheme for the H_2N-HN* to produce NH_3 is from the Enz pathway to Alt pathway.

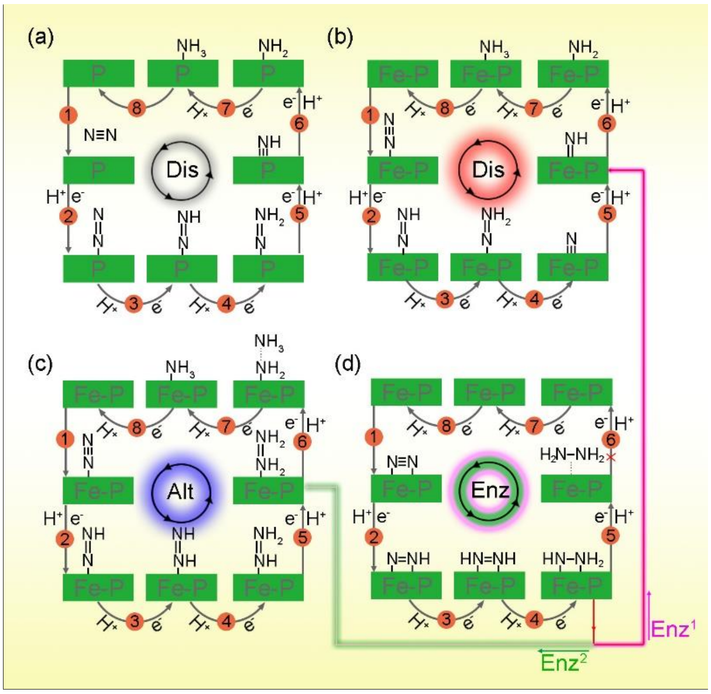

Figure 5. Schematic depiction of three mechanisms for N_2 reduction reaction: (a) P, (b-d), Fe-P. The Dis, Alt and Enz represent the Distal, Alternating and Enzymatic pathway, respectively.

We calculated the reaction energy at each step of each pathway, as shown in **Figure 6**a, and the relevant data are summarized in **Figure** S6. It is obvious that almost each step released energy except for the first step of P to adsorb N_2 molecule (0.44eV). The first step of the protonation in Fe-P was exothermic, which suggests that the N_2 was efficiently activated. Impressively, the N_2-to-NH_3 conversion can be carried out spontaneously in each pathway of Fe-P. It indicates that Fe-P is a promising electrocatalyst to convert the N_2 to NH_3. **Figure 6**b describes the process of the cleavage of N-N bond in each pathway. The detailed data was recorded in **Table S**3. We can find that the practically linear variation of N-N bond length before emitting the first NH_3, which reflects a gradual protonation process. The monotonically increasing relationship between N-N bond length and hydrogenation pathways revealed the potential ability of Fe-P to N_2-fixation.

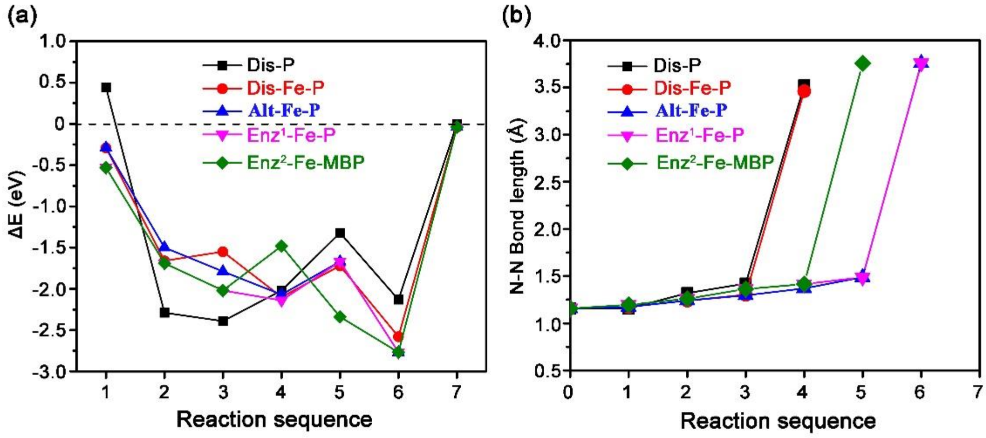

Figure 6. (a) Reaction energy and (b) N-N bond length in the N_2 reduction reaction process. The N-N bond length of the first dot in the reaction sequence 0 represents the free N_2.

To deep understand the superior catalytic performance of Fe-P on the N_2-fixation, we carried out charge population analysis. The data of all the charges was illustrated in **Tabel S**4. We divided the intermediates into three moieties: molecule for the bounded N, H atoms, P, and Fe atom, respectively.

It can be seen clearly that there was no electron transfer between molecule N_2 and P during its adsorption (**Figure** 7a), which agrees with previous discussion. In the following reduction reaction steps, the electron transfered from the P surface to the adsorbed molecule. For example, when the adsorbed N_2* was reduced to N_2H*, the formed N_2H* species can gain ca. 0.59 electrons from P, and about 1.12 electrons could be gained from P to N* and NH_3 species. Obviously, the moiety of P served as an electron donor during the N_2 reduction reaction process. After the Fe doping, the status of the charge variation have been recombined, and the P moiety can not only donate electrons but also gain electrons from other moieties. The Dis pathway of Fe-P can be found in **Figure 7**b. We found that the P moiety lost electrons in steps 1-2 and 4-5, but gained electrons from Fe moiety in steps 3 and 6-7. The Fe moiety started to lose electrons at the third step and served as a donor during the following reduction steps. It clearly demonstrate that the Fe moiety only acted as a donor offering electrons to other moieties, during the Alt-Fe-P (**Figure 7**c), Enz^1-Fe-P (**Figure 7**d) and Enz^2-Fe-P (**Figure 7**e) pathways. The P moiety mainly gained electrons from the Fe moiety, and only lost electrons in the third step in both Enz^1-Fe-P and Enz^2-Fe-P pathways. Additionally, we plotted the average charge variation in the five pathways, as illustrated in **Figure 7**f. We can find that P is an electron reservoir, and Fe is the active site for N_2-fixation and the transmitter for electron transfer. There is no doubt that the Fe doped P can be a novel catalyst for N_2 reduction reaction.

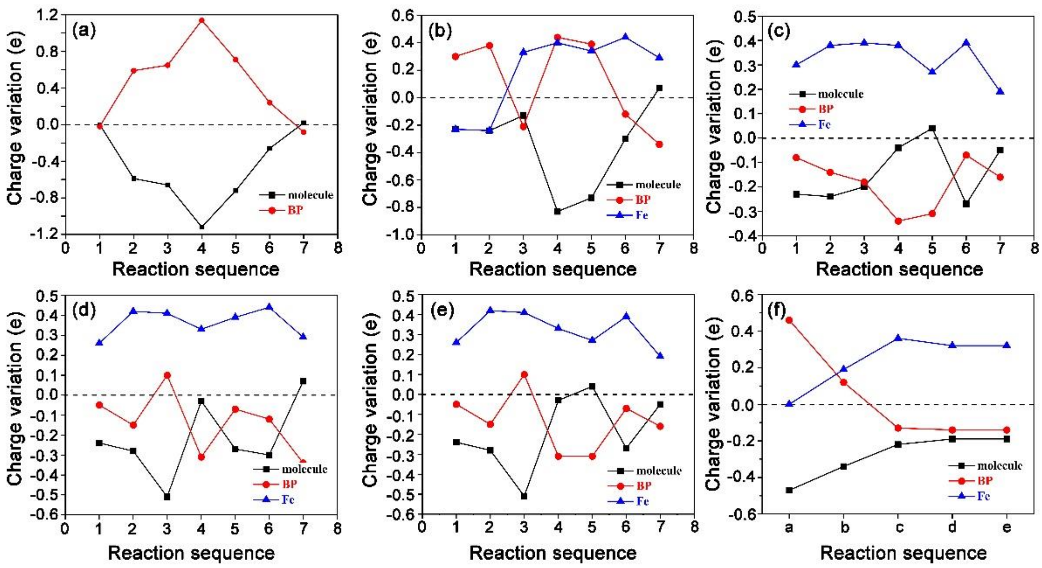

Figure 7. Charge variation of three moieties (molecule, P and Fe) along the pathway (a) Dis-P, (b) Dis-Fe-P, (c) Alt-Fe-P, (d) Enz^1-Fe-P, (e) Enz^2-Fe-P, respectively. (f) Mean charge variation of various moieties.

4 Conclusion

In summary, we have performed spin-polarized density functional theory to propose a new catalyst for N_2 reduction reaction at room temperature. The single atom (such as Fe) doped in the MP is the active site and plays a vital role in the N_2-to-NH_3 conversion. Our results suggest that the Fe-P catalyst is a great potential single atom catalyst with high efficiency catalyst for N_2 reduction reaction. This work reveals that the single atom (TM), collaborating with 2D layered materials (P) can be a novel candidate catalyst to N_2-fixation.

Acknowledgements

This work was supported by the National Natural Science Foundation of China (51302079), and the Natural Science Foundation of Hunan Province (2017JJ1008).

References

1. S. J. Ferguson, *Current Opinion in Chemical Biology*, 1998, **2**, 182-193.
2. J. Rittle and J. C. Peters, *Journal of the American Chemical Society*, 2016, **138**, 4243-4248.
3. J. N. Galloway, A. R. Townsend, J. W. Erisman, M. Bekunda, Z. Cai, J. R. Freney, L. A. Martinelli, S. P. Seitzinger and M. A. Sutton, *Science*, 2008, **320**, 889-892.
4. B. M. Hoffman, D. Lukoyanov, Z.-Y. Yang, D. R. Dean and L. C. Seefeldt, *Chemical Reviews*, 2014, **114**, 4041-4062.
5. K. C. Macleod and P. L. Holland, *Nature Chemistry*, 2013, **5**, 559-565.
6. T. A. Bazhenova and A. E. Shilov, *Coordination Chemistry Reviews*, 1995, **144**, 69-145.
7. B. A. Mackay and M. D. Fryzuk, *Cheminform*, 2004, **35**, 385-401.
8. I. A. Amar, R. Lan, C. T. G. Petit and S. Tao, *Journal of Solid State Electrochemistry*, 2011, **15**, 1845-1860.
9. S. Giddey, S. P. S. Badwal and A. Kulkarni, *International Journal of Hydrogen Energy*, 2013, **38**, 14576-14594.
10. V. Smil, *Scientific American*, 1997, **277**, 76-81.
11. C. J. M. van der Ham, M. T. M. Koper and D. G. H. Hetterscheid, *Chemical Society Reviews*, 2014, **43**, 5183-5191.
12. J. W. Erisman, M. A. Sutton, J. Galloway, Z. Klimont and W. Winiwarter, *Nature Geoscience*, 2008, **1**, 636-639.
13. A. Mittasch and W. Frankenburg, *Advances in Catalysis*, 1950, **2**, 81-104.
14. J. R. Jennings, *Catalytic Ammonia Synthesis*, Springer US, 1900.

15. Y. Miyake, K. Nakajima, H. Yu and Y. Nishibayashi, *European Journal of Inorganic Chemistry*, 2015, **2014**, 4273-4280.
16. J. S. Anderson, J. Rittle and J. C. Peters, *Nature*, 2013, **501**, 84-+.
17. R. R. Schrock, *Angewandte Chemie-International Edition*, 2008, **47**, 5512-5522.
18. E. E. Stueeken, R. Buick, B. M. Guy and M. C. Koehler, *Nature*, 2015, **520**, 666-U178.
19. J. Kim and D. C. Rees, *Biochemistry*, 1994, **33**, 389.
20. H.-P. Jia and E. A. Quadrelli, *Chemical Society Reviews*, 2014, **43**, 547-564.
21. D. V. Yandulov and R. R. Schrock, *Science*, 2003, **301**, 76-78.
22. K. Arashiba, Y. Miyake and Y. Nishibayashi, *Nature Chemistry*, 2011, **3**, 120-125.
23. K. Arashiba, E. Kinoshita, S. Kuriyama, A. Eizawa, K. Nakajima, H. Tanaka, K. Yoshizawa and Y. Nishibayashi, *Journal of the American Chemical Society*, 2015, **137**, 5666-5669.
24. T. J. Del Castillo, N. B. Thompson and J. C. Peters, *Journal of the American Chemical Society*, 2016, **138**, 5341-5350.
25. G. Ung and J. C. Peters, *Angewandte Chemie*, 2015, **54**, 532-535.
26. A. Banerjee, B. D. Yuhas, E. A. Margulies, Y. Zhang, Y. Shim, M. R. Wasielewski and M. G. Kanatzidis, *Journal of the American Chemical Society*, 2015, **137**, 2030-2034.
27. V. K. Shah and W. J. Brill, *Proceedings of the National Academy of Sciences of the United States of America*, 1977, **74**, 3249.
28. J. S. Anderson, M.-E. Moret and J. C. Peters, *Journal of the American Chemical Society*, 2013, **135**, 534-537.
29. Y. Tanabe and Y. Nishibayashi, *Coordination Chemistry Reviews*, 2013, **257**, 2551-2564.
30. M. M. Rodriguez, E. Bill, W. W. Brennessel and P. L. Holland, *Science*, 2011, **334**, 780-783.
31. S. Kattel and G. Wang, *Journal of Physical Chemistry Letters*, 2014, **5**, 452-456.
32. K. C. MacLeod, D. J. Vinyard and P. L. Holland, *Journal of the American Chemical Society*, 2014, **136**, 10226-10229.
33. J. S. Anderson, G. E. Cutsail, III, J. Rittle, B. A. Connor, W. A. Gunderson, L. Zhang, B. M. Hoffman and J. C. Peters, *Journal of the American Chemical Society*, 2015, **137**, 7803-7809.
34. R. Bjornsson, F. Neese, R. R. Schrock, O. Einsle and S. DeBeer, *Journal of Biological Inorganic Chemistry*, 2015, **20**, 447-460.
35. X.-F. Li, Q.-K. Li, J. Cheng, L. Liu, Q. Yan, Y. Wu, X.-H. Zhang, Z.-Y. Wang, Q. Qiu and Y. Luo, *Journal of the American Chemical Society*, 2016, **138**, 8706-8709.
36. S. Hu, X. Chen, Q. Li, F. Li, Z. Fan, H. Wang, Y. Wang, B. Zheng and G. Wu, *Applied Catalysis B: Environmental*, 2017, **201**, 58-69.
37. L. M. Azofra, C. Sun, L. Cavallo and D. R. Macfarlane, *Chemistry.*, 2017, **23**, 8275.
38. A.-J. Yang, D.-W. Wang, X.-H. Wang, J.-F. Chu, P.-L. Lv, Y. Liu and M.-Z. Rong, *Ieee Electron Device Letters*, 2017, **38**, 963-966.
39. C.-X. Wang, C. Zhang, J.-W. Jiang and T. Rabczuk, *Nanotechnology*, 2017, **28**.
40. J. Wang, D. Liu, H. Huang, N. Yang, B. Yu, M. Wen, X. Wang, P. K. Chu and X.-F. Yu, *Angewandte Chemie-International Edition*, 2018, **57**, 2600-2604.
41. X. Zhu, T. Zhang, Z. Sun, H. Chen, J. Guan, X. Chen, H. Ji, P. Du and S. Yang, *Adv Mater*, 2017, **29**.
42. S. K. Muduli, E. Varrla, Y. Xu, S. A. Kulkarni, A. Katre, S. Chakraborty, S. Chen, T. C. Sum, R. Xu and N. Mathews, *Journal of Materials Chemistry A*, 2017, **5**, 24874-24879.
43. S. Yang, F. Liu, C. Wu and S. Yang, *Small*, 2016, **12**, 4028-4047.
44. Y. Qiu, L. Xin, F. Jia, J. Xie and W. Li, *Langmuir*, 2016, **32**, 12569-12578.

45. J. P. Perdew, K. Burke and M. Ernzerhof, *Physical Review Letters*, 1996, **77**, 3865-3868.
46. R. Car and M. Parrinello, *Physical Review Letters*, 1985, **55**, 2471.
47. G. Wang, W. J. Slough, R. Pandey and S. P. Karna, *2d Materials*, 2015, **3**, 025011.
48. H. Liu, A. T. Neal, Z. Zhu, Z. Luo, X. Xu, D. Tománek and P. D. Ye, *Acs Nano*, 2014, **8**, 4033-4041.
49. Y.-Q. Le, J. Gu and W. Q. Tian, *Chemical Communications*, 2014, **50**, 13319-13322.
50. H. Xiao, Z.-S. Wu, L. Chen, F. Zhou, S. Zheng, W. Ren, H.-M. Cheng and X. Bao, *Acs Nano*, 2017, **11**, 7284-7292.
51. M. C. Hersam, J. Kang and J. D. Wood, *Journal*, 2017.
52. D. Hanlon, C. Backes, E. Doherty, C. S. Cucinotta, N. C. Berner, C. Boland, K. Lee, A. Harvey, P. Lynch and Z. Gholamvand, *Scientific Reports*, 2015, **6**, 8563.
53. L. Chen, G. Zhou, Z. Liu, X. Ma, J. Chen, Z. Zhang, X. Ma, F. Li, H. M. Cheng and W. Ren, *Advanced Materials*, 2016, **28**, 510.
54. T. Wang, W. Guo, L. Wen, Y. Liu, B. Zhang, K. Sheng and Y. Yin, *Journal of Wuhan University of Technology-Materials Science Edition*, 2017, **32**, 213-216.
55. W. Zhang and L. Zhang, *Rsc Advances*, 2017, **7**, 34584-34590.